Prethermal discrete time crystal in driven-dissipative dipolar systems

Saptarshi Saha [*] and Rangeet Bhattacharyya [†]
Department of Physical Sciences, Indian Institute of Science Education and Research Kolkata, Mohanpur 741246, West Bengal, India

(Received 11 August 2023; revised 23 November 2023; accepted 12 December 2023; published 11 January 2024)

Here we provide a theoretical framework to analyze discrete time-crystalline (DTC) phases in the dissipative dipolar systems subjected to a two-pulse excitation scheme. As a particular realization, we choose a quantum many-body system that exhibits prethermalization due to the presence of the quasiconserved quantities. The analysis uses a fluctuation-regulated quantum master equation, which captures the dissipative effects of the drive and dipolar coupling on the dynamics regularized by the thermal fluctuations. We find that the effects of such dissipation lend stability to the dynamics and are directly responsible for the robustness. Specifically, we find that longer fluctuation correlation time enhances the stability of DTC. We also obtain the lifetime of such a robust period-doubling response, a salient feature of the DTC phase, by varying several system parameters. Our results are in good agreement with the recent experimental findings in dipolar systems using nuclear magnetic resonance spectroscopy. Finally, we provide an estimate how the DTC performance degrades with temperature.

DOI: 10.1103/PhysRevA.109.012208

I. INTRODUCTION

In the recent past, several groups demonstrated, theoretically as well as experimentally, that driven quantum many-body systems exhibit a variety of exotic out-of-equilibrium phases [1–5], a prime example being the discrete time-crystalline (DTC) phase [6,7]. Wilczek originally proposed that a quantum system may exhibit a time-periodic echolike behavior through breaking of the continuous time-translation symmetry; however, the idea was later shown to be untenable [8,9]. Later Khemani, Else, and others proposed the concept of the DTC phase, which is characterized by breaking the discrete time-translation symmetry in the presence of a time-periodic Hamiltonian [10,11]. In this phase, the periodicity of any system observables is an integer multiple of the period of the drive Hamiltonian. Most commonly, DTCs exhibit a period doubling or a subharmonic response [11].

More recently, several groups experimentally demonstrated the existence of the DTC phase using nuclear magnetic resonance (NMR), trapped ions, and circuit QED systems [12–20]. One common feature for most of the experiments mentioned above is the application of external drives that contain two noncommuting Hamiltonians are applied in successive time steps. For examples, the experimental demonstrations by Choi *et al.* and Beatrez *et al.* use two-pulse schemes on driven dissipative dipolar systems [13,17]. We note that some groups also reported that the subharmonic response are stabilized by dissipation in DTC [18–20].

The two-pulse scheme consists of a spin-locking sequence along the x direction (the first drive) followed by a rotation along the y axis (the second drive) [13,17]. Choi *et al.* used an ensemble of dipolar coupled nitrogen-vacancy (NV) centers, whereas Beatrez *et al.* used dipolar coupled ^{13}C nuclear spins in a diamond to demonstrate such a novel subharmonic response. In both cases, it was theoretically observed that a critically slow thermalization or prethermalization occurred in the system, which plays a significant role in stabilizing the DTC phase under perturbations [21,22].

In general, for an isolated many-body system, the prethermalization in the presence of periodic drive is theoretically analyzed by Floquet theory (i.e., Floquet prethermalization) [22–27]. The effect of the Floquet heating in each cycle can be captured by the second-order contribution of the periodic drive [25]. In the presence of local interaction and high-frequency drive, such heating becomes exponentially slow, which results in a long-lived prethermal plateau in the system [28].

Although such systems are not perfectly isolated systems, they are weakly coupled with the external environment with a long relaxation time [22,29]. Recently, for such systems, we have provided a dynamical approach to describe the prethermalization in periodically driven dissipative dipolar systems [30,31]. We have used a recently proposed fluctuation-regulated quantum master equation (FRQME) [32], which successfully explained the interplay between the secular part of the on-resonant periodic drive and dipolar interaction that led to a prethermal phase. The dynamics is constrained by a set of quasiconserved quantities in this regime. Subsequently, the nonsecular interactions and system-bath interaction provide a very slow thermalization process. Thus, the second-order terms of the drive and dipolar interaction regulated by thermal fluctuations conveniently explain the effect of the Floquet heating in the system.

As the existing DTC phases in such systems are directly connected to the emerging long-lived prethermal order, such kind of robust period-doubling response is often known as prethermal discrete time crystal (PDTC). The term PDTC was first coined by Kypriandis *et al.* [16], however, the existence of such phases in the prethermal regime of periodically driven system was first predicted in a pioneer work by Else *et al.* [33].

[*]ss17rs021@iiserkol.ac.in
[†]rangeet@iiserkol.ac.in

We note that it has significant differences from the other types of DTC phases that appear in an open quantum system. For example, the boundary time crystal, measure-induced time crystal, where an effective mean-field QME has been implemented to obtain the persistent period-doubling oscillations in the thermodynamic limit of a many-body system [34–36]. On the other hand, PDTC has a finite lifetime, for example, in case of the dipolar coupled systems in the presence of periodic drive, the lower bound of the heating rate of the prethermal order is provided by the dipolar interaction [17]. In such cases, the maximum contribution is coming from the nearest-neighbor spins as the amplitude of the dipolar interaction falls off as r^{-3}, where r is the distance between the spin pairs. Beatrez *et al.* numerically show that a simplified model consisting of 14 spins can successfully mimic the experimental outcomes of PDTC in case of ^{13}C nuclear spins in diamonds [17].

Here, we provide an alternative prescription for the PDTC phase that emerged in dipolar coupled systems. Using FRQME, we obtain the existence of the stable DTC phase in such systems subjected to the two-pulse scheme as mentioned above. We also compare our analytical results with those experimental outcomes. In addition, we also check the robustness of such period-doubling response by varying the fluctuation correlation timescale, which is inversely proportional to the temperature.

We have arranged the paper in the following order. In Sec. II, we give a brief overview of the dissipative dipolar system subjected to a two-pulse scheme. The dynamics of the system for a two-spin ensemble case is discussed in Sec. III, where we separately discuss the dynamics under the spin-locking pulse in the x direction, and the θ rotation along the y direction. Using the dynamical equation of each pulse sequence, we show the emergence of the DTC phase in the same section. We further generalize our description for the N spin system in Sec. IV, and provide the numerical results for the robust DTC regime by varying several system parameters and comparing them with the existing experimental results. Finally, we briefly discuss the results and their implications in Sec. V and conclude in Sec. VI.

II. DESCRIPTION OF THE SYSTEM

We consider a dipolar coupled spin 1/2 system, which is weakly coupled with the external environment. We assume that the spin 1/2 particles are identical to each other. The free Hamiltonian of the system is written as, $\mathcal{H}_S = \sum_{i=1}^N \omega_\circ I_z^i$. Here, $\omega_\circ$ is the Zeeman frequency, N is the number of the spins, and $I_m = \sigma_m/2$. σ_m is the m component of the Pauli spin matrix [$m = \{x, y, z\}$]. $\mathcal{H}_{\rm dd}$ represents the dipolar interactions between the spin pairs, the analytical form of $\mathcal{H}_{\rm dd}$ is given by,

$$\mathcal{H}_{\rm dd} = \sum_{i,j=1}^{N} \frac{\mu_\circ}{4\pi r_{ij}^3}\gamma_a^2 \hbar(\vec{I}_i.\vec{I}_j - 3(\vec{I}_i.\hat{r})(\vec{I}_j.\hat{r})), \quad [i > j]. \quad (1)$$

Here, $\mu_\circ$ is the magnetic permeability constant, and γ_a is the gyromagnetic ratio.

Following the works by Beatrez *et al.* and Choi *et al.*, the system undergoes the two-pulse protocol [13,17]. A pictorial depiction of the two-pulse scheme is presented in Fig. 1. Initially, the spins are oriented along the z direction in the presence of the Zeeman field. A $\pi/2$ pulse along the y direction is applied to rotate the spins along the x direction. Therefore, the density matrix after that step is written as, $\rho_S|_{t\to 0} = |\psi\rangle\langle\psi|$. Here, $|\psi\rangle|_{t\to 0} = \otimes_{i=1}^N (|\uparrow\rangle_i + |\downarrow\rangle_i)/\sqrt{2}$. $|\uparrow\rangle$ and $|\downarrow\rangle$ are the eigenstate of the Zeeman basis. Next, a resonant periodic drive along the x direction is applied for a time duration of τ_1. In this period the dipolar interaction ($\mathcal{H}_{\rm dd}$) is also effective, such a pulse sequence is known as a spin-locking sequence in NMR [37]. The corresponding drive Hamiltonian is given by,

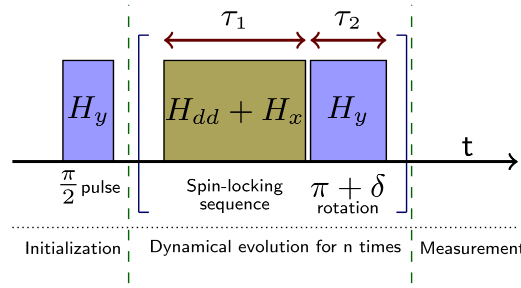

FIG. 1. The schematic diagram shows the experimental realization for demonstrating the DTC phase in the dissipative dipolar system. The initial state is prepared by using a $\pi/2$ pulse in the y direction. The two-drive protocol is given here. The spin-locking sequence is provided for τ_1 time, secondly, a $\theta = \pi + \delta$ rotation is given along y direction for a duration τ_2. The whole sequence, $\tau = \tau_1 + \tau_2$ is repeated for n times before measuring the final spectrum of $S[M_x(t)]$.

$$\mathcal{H}_x = \sum_{i=1}^{N} \omega_1 I_x^i \cos\omega_\circ t. \quad (2)$$

The dynamical equation of the reduced density matrix of the system (ρ_S) is given by the FRQME. The FRQME have been proposed and verified experimentally by Chakrabarti *et al.* in 2018 [32,38]. The analytical form of the FRQME in the interaction picture of the free Hamiltonian is given by [32],

$$\frac{d\rho_S}{dt} = -i\mathrm{Tr_L}\big[H_{\rm eff}(t), \rho_S \otimes \rho_{\rm L}^{\rm eq}\big]^{\rm sec} - \int_0^\infty d\tau \mathrm{Tr_L}\big[H_{\rm eff}(t), \big[H_{\rm eff}(t-\tau), \rho_S \otimes \rho_{\rm L}^{\rm eq}\big]\big]^{\rm sec} e^{-\frac{|\tau|}{\tau_c}}. \quad (3)$$

Here, we note that $0 < t < \tau_1$. $H_{\rm eff}(t)$ denotes the interaction representation of $\mathcal{H}_{\rm SL} + \mathcal{H}_x(t) + \mathcal{H}_{\rm dd}$. $\mathcal{H}_{\rm SL}$ is the system-bath coupling Hamiltonian, the detailed form of $\mathcal{H}_{\rm SL}$ is mentioned in our earlier work on spin locking [30]. τ_c is the fluctuation correlation timescale, and $\rho_{\rm L}^{\rm eq}$ is the equilibrium density matrices of the environment. The unique feature of the above Eq. (3) is the presence of the exponential kernel in the second-order terms that help calculate the dissipative effects of the coupling and drive, whereas a regular Born-Markov QME failed to explain such effects [39]. FRQME has been used as an efficient tool for analyzing several applications in NMR, quantum optics, and quantum information processing [40–44]. Here, we assume that the strength of drive and dipolar (ω_1, ω_d) is much stronger than the system-bath interaction ($\omega_{\rm SL}$), $\omega_1, \omega_d \gg \omega_{\rm SL}$. Such approximation is valid, when the system has a large relaxation time (T_1) [22].

Following the spin-locking sequence, a $\theta=\pi+\delta$ rotation is applied about the y direction. The corresponding Hamiltonian in the interaction picture is given by,

$$H_y = \omega_2 \sum_{i=1}^{N} I_y^i. \tag{4}$$

Here, $\omega_2 \tau_2 = \pi + \delta$. Here we assume that $\omega_2 \gg \omega_d$, so the effect of $\mathcal{H}_{\rm dd}$ is ignored in this time duration, and the required time τ_2 is usually small and hence the drive-induced dissipation is ignored [17]. The corresponding dynamical equation is given by the von Neumann-Liouville equation, which is written as,

$$\frac{d\rho_S}{dt} = -i[H_y, \rho_S]. \tag{5}$$

Here, we note that $\tau_1 < t < \tau_2$. To obtain the 2τ periodic response in the system, the total sequence, $\tau = \tau_1 + \tau_2$ is repeated n times [$n \in \mathcal{I}$]. We solved these equations (3) and (5) in the Liouville space, where $\hat{\rho}_S$ is a $N^2 \times 1$ column matrix and the Liouvillian ($\hat{\mathcal{L}}$) is a $N^2 \times N^2$ matrix. The corresponding dynamical equation in the Liouville space is given by, $d\hat{\rho}_S/dt = \hat{\mathcal{L}}\hat{\rho}_S$.

The final density matrix $\hat{\rho}_S(t)$ after the n cycle can be written as,

$$\hat{\rho}_S(t) = [e^{\hat{\mathcal{L}}_y \tau_2} e^{\hat{\mathcal{L}}_{\rm sp}\tau_1}]^n \hat{\rho}_S|_{t\to 0}. \tag{6}$$

Here, $\hat{\mathcal{L}}_y$ is the Liouvillian corresponding to the rotation along y direction and $\hat{\mathcal{L}}_{\rm SP}$ is the Liouvillian corresponding to the spin-locking sequence. The detailed analytical forms of $\hat{\mathcal{L}}_{\rm sp}$, $\hat{\mathcal{L}}_y$ are given in the next section.

III. DYNAMICS OF THE ENSEMBLE OF TWO-SPIN 1/2 PARTICLES

In this section, we are considering a simplified model of an ensemble of two dipolar coupled spin 1/2 particles connected to the thermal environment. As $\omega_d \propto 1/r^3$, the major contribution is coming from the nearest-neighbor spins. Therefore, such a simplified model can successfully describe the emergence of the prethermalization using the spin-locking sequence [30]. The analytical form of $\mathcal{H}_{\rm dd}$ can also be written in the spherical tensor notation for two-spin cases, which is given by, $\mathcal{H}_{\rm dd} = \sum_{m=-2}^{2}(-1)^m \omega_{d_m} \mathcal{T}_2^m$. Here, $\omega_{d_m} = (\mu_\circ \hbar \gamma^2/4\pi r^3)\ \mathcal{Y}_2^{-m}(\Theta, \phi)$, and $\mathcal{Y}_2^{-m}(\Theta, \phi)$ is the spherical harmonics of rank 2. (Θ, ϕ) are the polar and azimuthal angles of the orientation of the dipolar vector with respect to the direction of the Zeeman field. $\mathcal{T}_2^m$ is the irreducible spherical tensor (of rank 2 and order m).

A. Dynamics under spin-locking sequence

For the two-spin cases, in the interaction picture, both $\mathcal{H}_{\rm dd}$, $\mathcal{H}_x$ can written as a combination secular part and the nonsecular part. Here, $H_x^{\rm sec} = \omega_1 \sum_i I_x^i$ and $H_{\rm dd}^{\rm sec} = \omega_{d_0}\mathcal{T}_2^0 = \omega_{d_0}(2I_z^1 I_z^2 - I_x^1 I_x^2 - I_y^1 I_y^2)$. Similarly the nonsecular parts are written as, $H_{\rm dd}^{\rm n} = \sum_m (-1)^m \omega_{d_m} \mathcal{T}_2^m e^{-im\omega_\circ t}$ $[\forall m \neq 0]$, $H_x^{\rm n} = \sum_i \omega_1 (I_+^i e^{+2i\omega_\circ t} + I_-^i e^{-2i\omega_\circ t})$. Here, "sec" represents the secular part, and "n" represents the nonsecular part of the Hamiltonian. Using FRQME [Eq. (3)], the dynamical equation for this case is written as [30],

$$\begin{aligned}\frac{d\rho_S}{dt} &= \mathcal{L}_{\rm sp}[\rho_S(t)] \\ &= (\mathcal{L}_{\rm sec} + \mathcal{L}_{\rm nsec} + \mathcal{L}_{\rm SL})[\rho_S(t)], \quad [0 < t < \tau_1],\end{aligned} \tag{7}$$

where, $\mathcal{L}_{\rm sec}$, $\mathcal{L}_{\rm nsec}$, $\mathcal{L}_{\rm SL}$ are the contribution coming from the secular terms of drive and dipolar interaction, the nonsecular terms, and the system-bath coupling, respectively. Their detailed forms can be found in our earlier work [30]. $\mathcal{L}_{\rm sec}$ provides a decay rate for the system to reach the prethermal plateau. Similarly, $\mathcal{L}_{\rm nsec}, +\mathcal{L}_{\rm SL}$ provides the decay of the prethermal state to the final thermal state. We choose $\omega_1, \omega_d \gg \omega_{\rm SL}$ and $\omega_\circ \tau_c > 1$. Hence, $\mathcal{L}_{\rm sec}[\rho_S] > \mathcal{L}_{\rm nsec}[\rho_S] > \mathcal{L}_{\rm SL}[\rho_S]$. We also show the numerical results of the evolution of the x magnetization $[M_x(t)]$ for the four choices of τ_c. For decreasing τ_c, the prethermal plateau emerges at a much later timescale. Although, at a longer timescale, the decay terms ($\mathcal{L}_{\rm nsec}$, $\mathcal{L}_{\rm SL}$) become more effective, so the lifetime of the prethermal phase becomes shorter. The corresponding rate for reaching the prethermal plateau is proportional to τ_c and the decay rate of the plateau is $\frac{\tau_c}{1+(\omega_\circ \tau_c)^2}$, which implies that, for a long-lived prethermal plateau, one must have $\omega_\circ \tau_c \gg 1$ [30].

As we are interested in the dynamics of the systems up to the prethermalization, the contributions of the last two terms are ignored for the upcoming calculations. The analytical form of $\mathcal{L}_{\rm sec}[\rho_S]$ is given as,

$$\mathcal{L}_{\rm sec}[\rho_S] = -i[H_{\rm sec}, \rho_S] - \tau_c[H_{\rm sec}, [H_{\rm sec}, \rho_S]], \tag{8}$$

Here, $H_{\rm sec} = H_x^{\rm sec} + H_{\rm dd}^{\rm sec}$. We define $\hat{\mathcal{L}}_1 = -i[H_{\rm sec} \otimes \mathbb{I} - \mathbb{I} \otimes H_{\rm sec}^T]$. T denotes the transpose operator. Using this formula we get, $\hat{\mathcal{L}}_{\rm sp} = \hat{\mathcal{L}}_1 + \tau_c \hat{\mathcal{L}}_1 \times \hat{\mathcal{L}}_1$. We analyze Eq. (7) using a set of symmetric and antisymmetric observables, for which we have.

$$\rho_S(t) = \sum_{\alpha,\beta} A_{\alpha\beta}(t) I_\alpha \otimes I_\beta, \tag{9}$$

where, α, $\beta \in \{x, y, z, d\}$, and $I_d = 2\times 2$ identity matrix. $M_i = A_{id} + A_{di}, M_{ii} = A_{ii}, M_{ij} = A_{ij} + A_{ji}\ \forall i \neq j$, and $i, j \neq d$. As the initial condition belongs to the symmetric observables, the evolution of the antisymmetric observables is negligible in comparison to the symmetric observables. The detailed dynamical equations in terms of observables are shown in Appendix A. In terms of symmetric observables, the dynamics can be divided into two subgroups $\{M_x, M_{yy}, M_{zz}, M_{yz}\}$ and $\{M_z, M_y, M_{xz}, M_{xy}\}$. For the given initial condition, the dynamics is confined only within the first subgroup. There exist several conserved quantities in the first subgroup, which are written as, $3\omega_d \dot{M}_{zz} + \omega_1 \dot{M}_x = 0$, $\dot{M}_{yy} + \dot{M}_{zz} = 0$, and $\dot{M}_{xx} = 0$ [30]. The existence of such conserved quantities ensures that, if initially, any one of the observables from the first group is nonzero, then they have finite values at the prethermal state. The solution of $M_x(t)$ by solving the above Eq. (8) for $M_x|_{t\to 0} = M_\circ$ is given as,

$$M_x^{\mathrm{pre}}(M_\circ, t) = M_\circ\left(\frac{4\omega_1^2}{\kappa_1^2} + \frac{9}{4}\frac{\omega_{d_0}^2}{\kappa_1^2}\cos(\kappa_1 t)e^{-\kappa_1^2 t\tau_c}\right). \quad (10)$$

Here, $\kappa_1^2 = 4\omega_1^2 + \frac{9}{4}\omega_{d_0}^2$. The above solution [Eq. (10)] signifies that $M_x^{\mathrm{pre}}(M_\circ, t)$ will reach a steady state, and the steady-state value is given as $M_x^{\mathrm{pre}}|_{t\to\infty} = M_\circ\frac{4\omega_1^2}{\kappa_1^2}$. We note that, in the limit $\omega_\circ\tau_c > 1$, and $\omega_1, \omega_d \gg \omega_{\mathrm{SL}}$, our numerical results [Fig. 2(a)] matches well with the experimental evidences by Beatrez *et al.* [22]. In the next sections, we show that such a long-lived prethermal plateau helps to stabilize the DTC phase.

B. Dynamics under the rotation along the *y* direction

We note that the rotation along the y direction occurs for a short duration, so, no heating occurs in this time duration. In other words, the effects of the dissipators are negligible during this period. Therefore, the dynamics is adequately described by the first-order process. Here, $H_y = \omega_2\sum_{i=1}^2 I_y^i$. To obtain the existence of the DTC phase, we are only interested in the dynamics of $M_x(t)$. The solution of Eq. (5) in terms of $M_x(t)$ is written as,

$$M_x^{\mathrm{rot}}(t) = M_1\cos(\omega_2 t), \quad M_z^{\mathrm{rot}}(t) = M_1\sin(\omega_2 t). \quad (11)$$

Here, $M_x^{\mathrm{rot}}|_{t\to 0} = M_1$. We define $\hat{\mathcal{L}}_y = -i[H_y\otimes\mathbb{I} - \mathbb{I}\otimes H_y^T]$.

C. Emergence of the DTC phase

To study the emergence of the DTC phase in the two-spin ensemble, we provide the analytical solution of $M_x(t)$ up to 2τ time period by solving Eq. (6). In experiments, drive strength is taken to be stronger than the dipolar interaction ($\omega_1 > \omega_d$). Such consideration leads to the negligible decay of $M_x(t)$ in the transient phase [13]. In this limit, the evolution of M_{zz}, M_{yy}, M_{yz} is negligible with respect to $M_x(t)$, which is shown in Appendix A. For the initial condition $M_x|_{t\to 0} = 1$, the solution of $M_x(t)$ at time τ_1 is given as,

$$M_x(\tau_1) = M_x^{\mathrm{pre}}(1, \tau_1), \quad M_z(\tau_1) = 0. \quad (12)$$

After the rotation, the solution is given by,

$$M_x(\tau) = M_x^{\mathrm{pre}}(1, \tau_1)\cos\theta, \quad M_z(\tau) = M_x^{\mathrm{pre}}(1, \tau_1)\sin\theta. \quad (13)$$

Here, $\theta = \omega_2\tau_2$. Similarly, after a time $\tau + \tau_1$, the solution is,

$$\begin{aligned} M_x(\tau+\tau_1) &= M_x^{\mathrm{pre}}\big[M_x^{\mathrm{pre}}(1, \tau_1), \tau_1\big]\cos\theta, \\ M_z(\tau+\tau_1) &= M_z^{\mathrm{pre}}\big[M_x^{\mathrm{pre}}(1, \tau_1), \tau_1\big]\sin\theta. \end{aligned} \quad (14)$$

Finally after the 2τ time period, the analytical expression of $M_x(2\tau)$ is written as,

$$\begin{aligned} M_x(2\tau) =& M_x^{\mathrm{pre}}\big[M_x^{\mathrm{pre}}(1, \tau_1), \tau_1\big]\cos^2\theta \\ &+ M_z^{\mathrm{pre}}\big[M_x^{\mathrm{pre}}(1, \tau_1), \tau_1\big]\sin^2\theta. \end{aligned} \quad (15)$$

Here, the form of $M_z^{\mathrm{pre}}(\alpha, t)$ is obtained by solving the dynamical equations of the other subgroup $\{M_z, M_y, M_{xz}, M_{xy}\}$, which is shown in Appendix A.

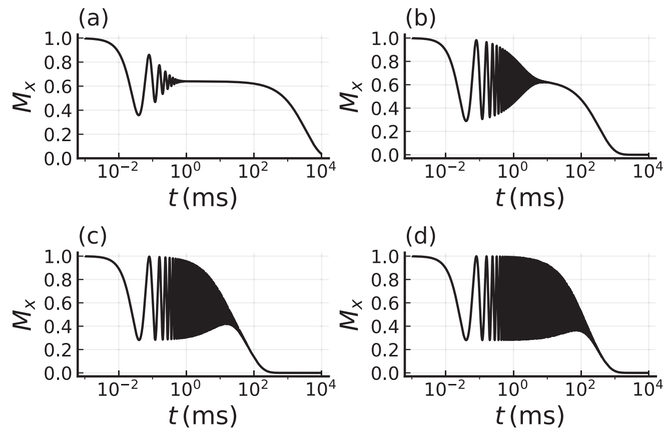

FIG. 2. Plots of M_x versus time are shown in (a), (b), (c), and (d) for the four choices of τ_c, which are 10^{-3} ms, 10^{-4} ms, 10^{-5} ms, and 10^{-6} ms, respectively. Here, $\omega_2\tau_2 = 0$. The value of the fixed parameters are given as, $\omega_1 = 2\pi\times 5$ kHz, $\omega_d = 2\pi\times 5$ kHz, $\omega_\circ = 2\pi\times 10^4$ kHz, and $\omega_{\mathrm{SL}} = 10^{-1}$ kHz. We note that, when $\tau_c > 1/\omega_\circ$, there is a finite lifetime of the prethermal plateau, whereas, for $\tau_c < 1/\omega_\circ$, the system directly thermalizes, so, there is no existence of the prethermal plateau.

1. *Solution for θ = π*

Putting $\theta = \pi$, in the above solutions, we get,

$$\begin{aligned} M_x(0) &= 1, \\ M_x(\tau_1) &= M_x^{\mathrm{pre}}(1, \tau_1), \\ M_x(\tau) &= -M_x^{\mathrm{pre}}(1, \tau_1), \\ M_x(\tau+\tau_1) &= -M_x^{\mathrm{pre}}\big[M_x^{\mathrm{pre}}(1, \tau_1), \tau_1\big], \\ M_x(2\tau) &= M_x^{\mathrm{pre}}\big[M_x^{\mathrm{pre}}(1, \tau_1), \tau_1\big]. \end{aligned} \quad (16)$$

In the above Eq. (16), we show that, in every time period τ, the sign of M_x is reversed. Therefore, $M_x(t)$ comes to the same phase at every 2τ time period, which signifies that the system shows the period-doubling response. On the other hand, $M_z(t)$ remains zero throughout the evolution. For increasing the values of ω_d, we note that κ_1^2 increases, which signifies that the value $M_x^{\mathrm{pre}}(1, \tau_1)$ decreases in every cycle, therefore such period-doubling response becomes short lived. It was previously reported that the melting of DTC order is proportional to the square of the interaction strength [17]. In our case, we find that $\kappa_1^2 \propto \omega_d^2$, which supports the existing experimental results. Hence, for a robust DTC regime, we need $\omega_1 > \omega_d$.

2. *Solutions for θ = π + δ, with δ/π → 0*

To obtain the stability of the DTC phase, we apply a perturbation (δ) in the π rotation. In such cases, we note that, $\cos(\pi+\delta) = -1$, $\sin(\pi+\delta) = -\delta$. The solution is given by,

$$\begin{aligned} M_x(0) &= 1, \\ M_x(\tau_1) &= M_x^{\mathrm{pre}}(1, \tau_1), \quad M_z(\tau_1) = 0, \\ M_x(\tau) &= -M_x^{\mathrm{pre}}(1, \tau_1), \quad M_z(\tau) = -\delta M_x^{\mathrm{pre}}(1, \tau_1) \\ M_x(\tau+\tau_1) &= -M_x^{\mathrm{pre}}\big[M_x^{\mathrm{pre}}(1, \tau_1), \tau_1\big], \\ M_z(\tau+\tau_1) &= -\delta M_z^{\mathrm{pre}}\big[M_x^{\mathrm{pre}}(1, \tau_1), \tau_1\big] \\ M_x(2\tau) &= M_x^{\mathrm{pre}}\big[M_x^{\mathrm{pre}}(1, \tau_1), \tau_1\big] \\ &\quad + \delta^2 M_z^{\mathrm{pre}}\big[M_x^{\mathrm{pre}}(1, \tau_1), \tau_1\big]. \end{aligned} \quad (17)$$

In the above solutions [Eq. (17)], the 2τ periodicity is absent due to the presence of the extra term in $M_x(2\tau)$, the period-doubling response is. Such a response can be retrieved if $\delta^2 \to 0$ or $M_z^{\text{pre}}(M_x^{\text{pre}}(1, \tau_1), \tau_1) \to 0$. In Appendix A, we show the plot of $M_z^{\text{pre}}(t)$ for various choices of τ_1, and τ_c. We note that, $M_z^{\text{pre}}(M_\alpha, t)$ decays faster for higher values of τ_1, and τ_c. Therefore, higher τ_1 and lower δ are suitable conditions for observing the DTC phase in the system, which matches with the previous experimental results [13].

For, $\omega_1 > \omega_d$, the expressions of $M_z^{\text{pre}}(M_\alpha, t)$ is given as,

$$M_z^{\text{pre}}(M_\alpha, t) = M_\alpha \cos(\omega_1 t) e^{-\omega_1^2 \tau_c t}. \tag{18}$$

Therefore, for higher values of τ_c, the effect of the extra term of $M_x(2\tau)$ in Eq. (17) can be neglected so, the DTC response is robust in this regime. For the generalization of our theoretical results for the two-spin ensemble, we inspect a many-spin dipolar coupled ensemble in the next section. We also study the existence of a stable DTC regime in the presence of a two-pulse sequence by varying ω_1, ω_d, τ_1, δ, τ_c, n and N.

IV. DYNAMICS OF THE ENSEMBLE OF N SPIN 1/2 PARTICLES

Here, we consider an ensemble of N-spin dipolar coupled systems weakly coupled to the environment. For simplicity, we model the individual dipolar coupling between the spin pairs by an averaged coupling amplitude. Due to such averaging, the coupling amplitude is always lower than the coupling between the nearest-neighbor interaction. Following the works by Lacelle *et al.*, in case of N-spin systems, the number of distinct spin pairs are $N(N-1)/2$, so the averaged coupling amplitude is given by, $\omega_d \propto |\omega_{d_{ij}}| 2N/[N(N-1)]$ [45]. Here, $|\omega_{d_{ij}}|$ is the nearest-neighbor coupling amplitude. The advantage of the above simplification is given below. The secular Hamiltonian, $H_x^{\text{sec}} + H_{\text{dd}}^{\text{sec}}$, and the rotation Hamiltonian H_y commutes with $\mathbf{J}^2$ operator, the form of the operator $\mathbf{J}_i$ is defined as,

$$\vec{\mathbf{J}} = \sum_{i=1}^{N} \sum_{a=x,y,z} \frac{\vec{\sigma}_{ai}}{2}. \tag{19}$$

It is also known as the total angular momentum operator or the collective operator. Therefore, those Hamiltonians can be written by using the collective basis, $|J, m\rangle$. Here, $J_{\max} = N/2$, and $-N/2 \leqslant m \leqslant N/2$. The representation of the Hamiltonians is given by,

$$\begin{aligned} H_{\text{dd}}^{\text{sec}} &= \omega_d\left(2J_z^2 - J_x^2 - J_y^2\right), \\ H_x^{\text{sec}} &= \omega_1 J_x, \\ H_y &= \omega_2 J_y. \end{aligned} \tag{20}$$

The matrix elements of the collective operators in the $|J, m\rangle$ basis are given below,

$$\begin{aligned} J_z &= m\delta_{J',J}\delta_{m',m} \\ J_\pm &= \sqrt{(J \mp m)(J \pm m + 1)}\delta_{J',J}\delta_{m',m\pm1}. \end{aligned} \tag{21}$$

Here, $J_x = J_+ + J_-$ and $J_y = (J_+ - J_-)/i$. We note that, using the collective operators, $\hat{\mathcal{L}}_{\text{sp}}$ and $\hat{\mathcal{L}}_y$ can be written in the block-diagonal form. Therefore, if the initial condition belongs to the particular block, the dynamics remain confined in that particular block. We choose the initial state to be the eigenstate corresponding maximum eigenvalue of J_x, where $J = N/2$, so the dynamics is confined in the principal J block. We also note that, for the atom number N, the size of the principal block is $(N+1)\times(N+1)$, whereas, in the Zeeman basis, no such block structure arises and the size of the Hilbert space is $N^2 \times N^2$. Such reduction of the dimensions in this case has several numerical benefits.

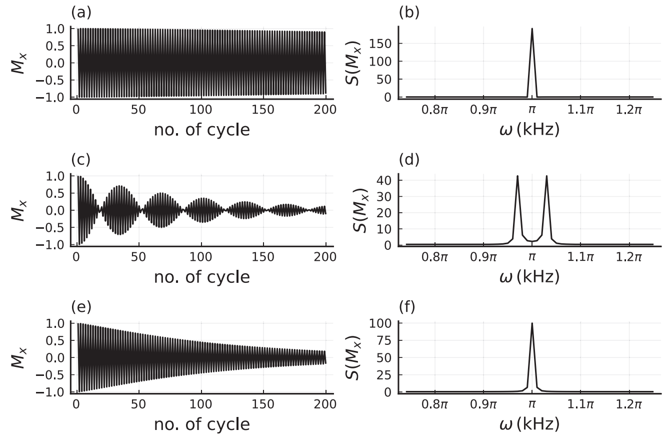

FIG. 3. Plots of M_x versus the number of cycles are shown in (a), (c), (e) and their corresponding Fourier transform, $S(M_x)$ versus ω are shown in (b), (d), and (f). The value of the fixed parameters are given as, $\omega_1 = 2\pi \times 25$ kHz, $\omega_d = 2\pi \times 0.1$ kHz, $\tau_c = 10^{-3}$ ms, $N = 15$, and $n = 200$. For the top plot [(a), (b)], $\omega_1\tau_1 = 2\pi \times 0.02$, $\omega_2\tau_2 = \pi$. For the middle plot [(c), (d)], $\omega_1\tau_1 = 2\pi \times 0.02$, $\omega_2\tau_2 = 1.03\pi$. For the bottom plot [(e), (f)], $\omega_1\tau_1 = 2\pi$, $\omega_2\tau_2 = 1.03\pi$. The period doubling occurs for the upper plot [(b)] as the peak of the Fourier spectra appears at $\omega = \pi$. A small increase in $\omega_2\tau_2$ destroys the 2τ periodic response [shown in (d)], which can be retrieved with a higher decay rate for a significant increment of $\omega_1\tau_1$ [shown in (f)]. In plots showing spectra in (b), (d), and (f), the y axis is in arbitrary units.

We note that along with $\langle \mathbf{J}^2 \rangle$, there exist another quantity for the evolution under $\mathcal{L}_{\text{sp}}$, which is given by,

$$\frac{d}{dt}\left(\omega_1 \langle J_x \rangle + 3\omega_d \langle J_z^2 \rangle\right) = 0. \tag{22}$$

The above Eq. (22) is the natural extension of the two-spin ensemble case, which ensures that $\langle J_x \rangle$ will reach a nonzero prethermal state. Next, we study the emergence of the DTC phase in the system using the above-mentioned prethermal state. Finding the dynamical equation for the many-spin systems is cumbersome, as there exist several operators in the dynamics. Therefore, we numerically solve Eq. (6) for $N = 15$ and find $M_x(t)$, and we also obtain the regime of stable DTC phase by varying the relevant parameters [ω_1, ω_d, δ, τ_1, n, N, and τ_c]. For the next part of the calculation, we denote $\frac{\langle J_x(t) \rangle}{(N/2)}$ as $M_x(t)$.

We calculate $M_x(t)$ and its spectrum for the initial condition $M_x|_{t\to 0} = 1$ and plot in Fig. 3. For a fixed ω_d, ω_1, n, and τ_c, when $\omega_2\tau_2 = \pi$ and $\omega_1\tau_1 = 2\pi \times 0.02$, we confirm a subharmonic response. For $\omega_2\tau_2 = \pi$, the x magnetization flipped from $\hat{x}$ to $-\hat{x}$ in each cycle, therefore the spectrum has a single

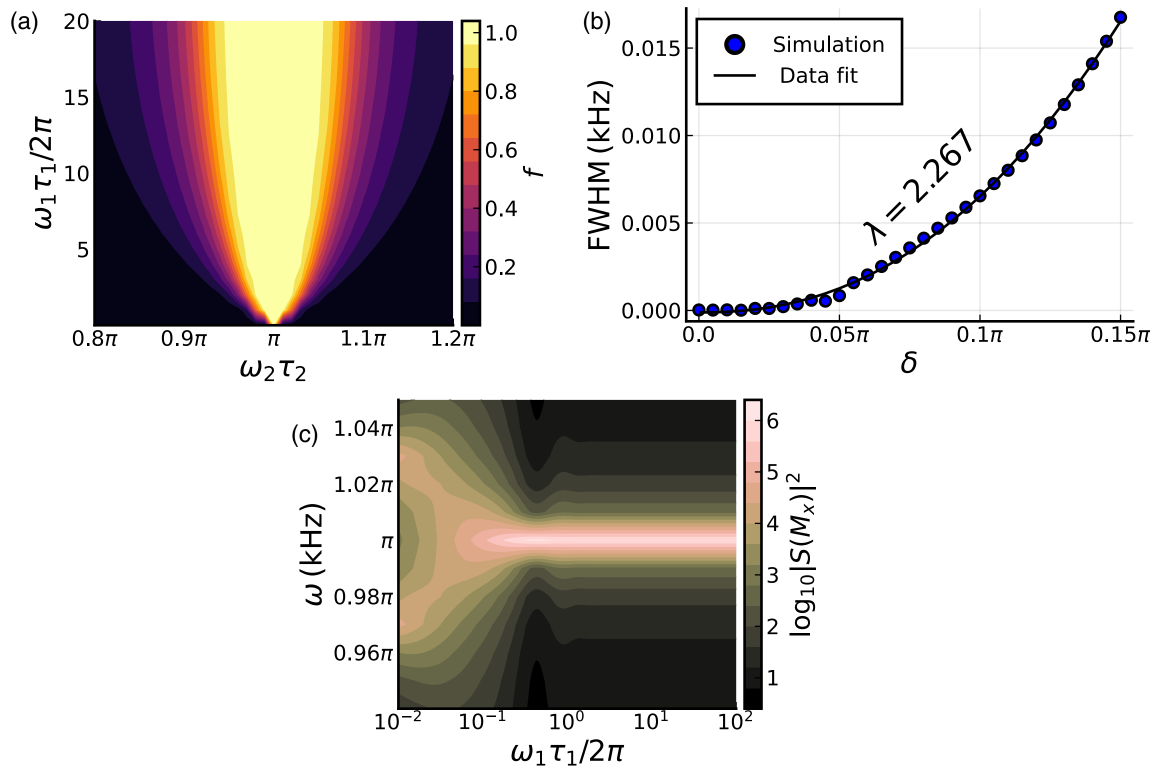

FIG. 4. (a) shows the contour plot of the crystalline fraction (f) as a function of dimensionless quantities $\omega_1\tau_1$ and $\omega_2\tau_2$. The list of fixed parameters are given here, $\omega_1 = 2\pi \times 100$ kHz, $\omega_d = 2\pi \times 0.1$ kHz, $\tau_c = 10^{-5}$ ms, $N = 15$, and $n = 200$. We note that the DTC phase is more robust for lower values of $|\omega_2\tau_2 - \pi|$ and higher values of $\omega_1\tau_1$. Here $f = 0.1$ is defined as the phase boundary. To understand the dependence of δ on the decay rate of the DTC phase, we plot the FWHM of the spectrum of $M_x(t)$ as a function of dimensionless δ and also fit the plot with $p_2(\delta) = a + b\times\delta^\lambda$ in (b). The list of the fixed parameters are given as, $\omega_1 = 2\pi \times 50$ kHz, $\omega_d = 2\pi \times 0.1$ kHz, $\tau_c = 10^{-3}$, $N = 15$, and $n = 200$. The fitting parameters are chosen as $a = 1.147\times10^{-4}$, $b = 1.227$, and $\lambda = 2.267$. Hence, for higher δ, such period-doubling response decays much faster. (c) shows the contour plot of $|S(M_x)|^2$ as a function of $\omega_1\tau_1$ and ω, for a fixed drive strength ω_1. The list of fixed parameters is given here, $\omega_1 = 2\pi \times 100$ kHz, $\omega_d = 2\pi \times 0.1$ kHz, $\omega_2\tau_2 = 1.03\pi$, $\tau_c = 10^{-3}$ ms, $N = 15$, and $n = 200$. For lower values of τ_1, there is no existence of the DTC phase, as two peaks appear at $\omega = \pi + \delta$. As, we increase τ_1, a robust DTC regime can be found for higher values of τ_1. However, for a very high τ_1, due to the presence of nonsecular terms and system-bath coupling, such robustness dies out.

peak at a position $\omega = \pi$ (top curve in Fig. 3). Next, we study the stability of the 2τ response by varying the experimental parameters τ_1 and δ. For the same τ_1, if $\delta = 0.03\pi$, the 2τ periodicity vanishes, and we get two peaks very close to ω, $\omega = \pi \pm \delta$. Such period-doubling response can be retrieved with a larger τ_1 (100 times than the previous one). Therefore, our result suggests that lower δ and higher τ_1 are desirable for observing the DTC phase. This numerical finding matches with our theoretical calculation for two-spin ensemble calculations, where for large τ_1, the extra term in Eq. (17) vanishes, so the period-doubling response can be retrieved. Although for a very high τ_1, the other terms $\mathcal{L}_{\rm nsec} + \mathcal{L}_{\rm SL}$ become effective, which provide a decay in $M_x(t)$, therefore the prethermal phase is destroyed. As a result, the DTC phase also vanishes for a very high τ_1 regime.

Following the works by Choi *et al.*, we define the crystalline fraction (f) as [13],

$$f = \frac{|S(\omega = \pi)|^2}{\sum_\omega |S(\omega)|^2}. \tag{23}$$

We also show a contour plot of crystalline fraction (f) as a function of dimensionless quantities $\omega_2\tau_2$ and $\omega_1\tau_1$ to capture the regime of the DTC phase in the system. The plot of f clearly shows the dependence of δ and τ_1 on the DTC phase. The stable regime is shown in the yellow regime of the contour plot in Fig. 4(a), which also matches with earlier experimental results [13]. Here $f = 0.1$ is defined as the phase boundary, so, below $f = 0.1$, there is a smooth crossover from the DTC phase to the non-DTC phase. We note that the period-doubling response vanishes quickly for increasing δ. To find the dependence of δ on the decay rate, we numerically plot the spectrum of $M_x(t)$ and fit them with the following Lorentzian function, $f_L(\omega) = \frac{p_1\times p_2}{p_2^2+(\omega-\pi)^2}$. Here p_1, p_2 is the fitting parameters. Especially, p_2 represents the width of the spectrum, which is also proportional to the full width half-maximum (FWHM). We numerically calculate p_2 for different choice of δ and fit with the following function, $p_2(\delta) = a + b\times\delta^\lambda$, here a, b, λ are the fitting parameters. The comparison between the numerical and data fitting is shown in Fig. 4(b). Our result shows that $\lambda = 2.267$, which matches well with the experimental result by Beatrez *et al.* [17].

For $\omega_2\tau_2 = 0$, the solution of the dynamical equation [Eq. (6)] shows the prethermalization in the system as $M_x(t)$ reaches a quasisteady state [Eq. (10)]. Therefore, in Fig. 5(a), prethermalization occurs in the blue regime near the $\omega_2\tau_2 = 0$. On the other hand, the system reaches the DTC

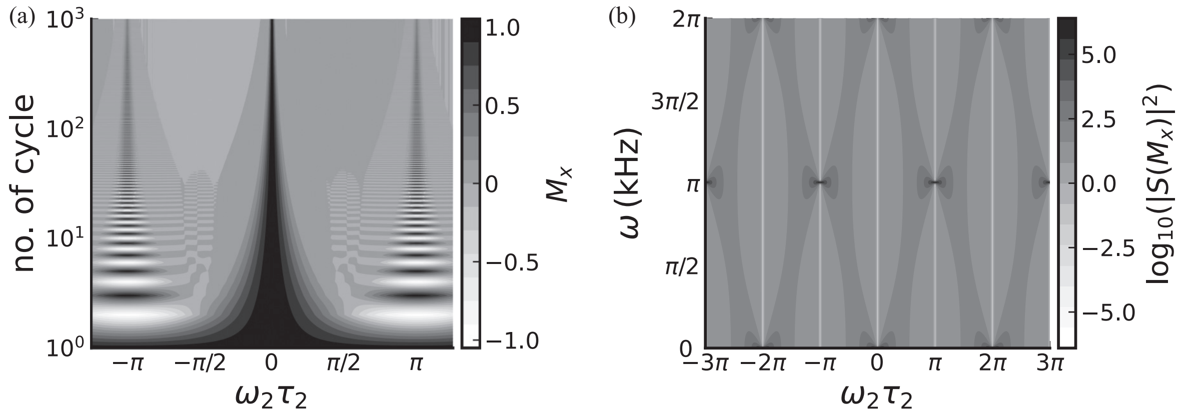

FIG. 5. (a) shows the contour plot of M_x as a function of dimensionless $\omega_2\tau_2$ and the no. of cycle (n). The list of fixed parameters is given here, $\omega_1 = 2\pi\times50$ kHz, $\omega_d = 2\pi\times0.1$ kHz, $\tau_c = 10^{-3}$ ms, $\omega_1\tau_1 = 2\pi$, $N = 15$, and $n = 1000$. The black region around $\omega_2\tau_2 = 0$ is known as the prethermal phase. The alternative black and white stripes around $\omega_2\tau_2 = \pm\pi$ shows the existence of the stable DTC phase up to $n = 500$. (b) shows the contour plot of $|S(M_x)|^2$ as a function of $\omega_2\tau_2$ and ω. The list of fixed parameters is given here, $\omega_1 = 2\pi\times50$ kHz, $\omega_d = 2\pi\times0.1$ kHz, $\tau_c = 10^{-3}$ ms, $\omega_1\tau_1 = 2\pi\times2$, $N = 15$, and $n = 200$. The Fourier peak around $\omega = \{0,\ 2\pi\}$ arises due to the presence of the prethermal phase; similarly, the peaks around $\omega = \pi$ denote the emergence of the DTC phase.

phase around $\omega_2\tau_2 = \pm\pi$. The alternative dark bands occur due to the flipping of M_x at each cycle, $[\mathrm{sgn}[(M_x)_{2n+1}] = -\mathrm{sgn}[(M_x)_{2n}]]$, which shows a robust subharmonic response around $\omega_2\tau_2 = \pm\pi$. Our calculation also shows that such a period-doubling response is robust up to 500 cycles.

To confirm the existence of the DTC phase in the system, we also provide a contour plot of the spectrum of M_x in Fig. 5(b). The prethermal phase occurs when $\omega_2\tau_2 = 2N\pi$, $\{N \in I\}$. Therefore, the Fourier peak arises at $\omega = 0,\ 2\pi$ for that particular values of $\omega_2\tau_2$, which signifies that the applied drive and the response have the same periodicity at the prethermal phase. From Fig. 5(a), we find that DTC phase occurs at $\omega_2\tau_2 = \pm\pi$, similarly the Fourier peaks in Fig. 5(b) arise at $\omega = \pi$ for $\omega_2\tau_2 \approx \pm(2N+1)\pi$. The results corresponding to Figs. 5(a), 5(b) are in agreement with the experimental observation by Beatrez *et al.* [17].

In our dynamical equation [Eq. (6)], τ_c plays an important role. To demonstrate the τ_c dependence of the DTC phase, We also plot $M_x(t)$ and its Fourier transform $\mathcal{S}[M_x(t)]$. For low values of τ_c, there is no existence of 2τ periodicity, but for changing the value of τ_c from 10^{-7} ms to 10^{-3} ms, such a novel response is retrieved, which is shown in Fig. 6. Although, τ_c cannot be increased infinitely as it has a cutoff, which is determined by, $\omega_1\tau_c < 1$. Beyond that limit, the perturbation theory breaks down. The numerical results also match with the analytical calculations, as for higher values of τ_c, the effect of the extra term of $M_x(2\tau)$ in Eq. (17) can be neglected.

We find that the roles of τ_1 and τ_c are complementary. It is well known that τ_c is inversely proportional to the temperature [38]. Hence, at lower temperatures, the effect of the imperfect rotation would be diminished, and the subharmonic response could be restored. We also show a contour plot of $|S(M_x)|^2$ as a function of τ_c and ω in Fig. 7(a), which shows that for decreasing τ_c, the peak at $\omega = \pi$ becomes broader and after a certain value, the DTC phase vanishes as instead of one peak at $\omega = \pi$, we got two peaks at $\omega = \pi \pm \delta$. Therefore, the 2τ periodic response vanishes for lowering τ_c. To find the rate of broadening, we follow a similar protocol, which we did numerically for $p_2(\delta)$ vs δ. In this case, we get $p_2(\tau_c) \propto \tau_c^{-1}$, which shows in Fig. 7(b).

To find the dependency of ω_1, ω_d on the robust DTC phase, we also show a contour plot of $\log_{10}|S(M_x)|^2$ as a function of ω_1 (for fixed ω_d) and ω_d (for fixed ω_1) in Figs. 8(a), 8(b) respectively. Two plots show the exactly opposite behavior. We note that, $M_x^{\mathrm{pre}} \propto (\frac{\omega_1}{\omega_d})^2$, and a higher value of M_x^{pre} is required for a stable DTC phase. For increasing ω_1, and for

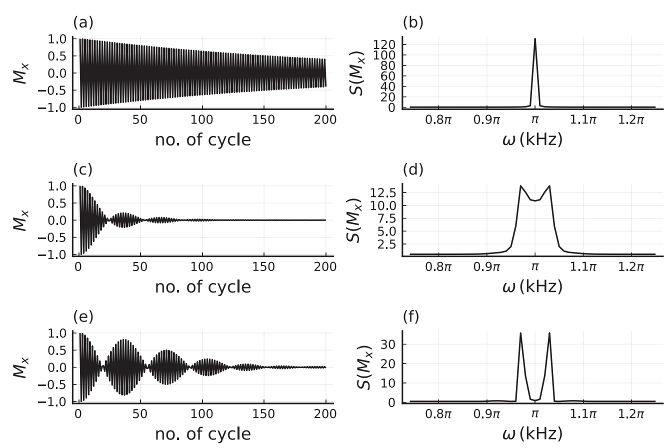

FIG. 6. Plot of M_x versus the number of cycles are shown in (a), (c), (e) and their corresponding Fourier transforms, $S(M_x)$ versus ω are shown in (b), (d), and (f). The chosen parameters are $\omega_1 = 2\pi\times125$ kHz, $\omega_d = 2\pi\times0.1$ kHz, $n = 200$, $\omega_1\tau_1 = 2\pi\times2$, $N = 15$, and $\omega_2\tau_2 = 1.03\pi$. For the top plot [(a), (b)], $\tau_c = 10^{-3}$ ms. For the middle plot [(c), (d)], $\tau_c = 10^{-5}$ ms. For the bottom plot [(e), (f)], the value of $\tau_c = 10^{-7}$ ms. We note that the intensity of the spectrum is maximum for $\tau_c = 10^{-3}$ ms, and by decreasing τ_c, such intensity is also suppressed and for $\tau_c = 10^{-7}$, the intensity is nearly zero. The above plots signifies that lowering τ_c results in the decay of robust 2τ response in the system. In plots showing spectra in (b), (d), and (f), the y axis is in arbitrary units.

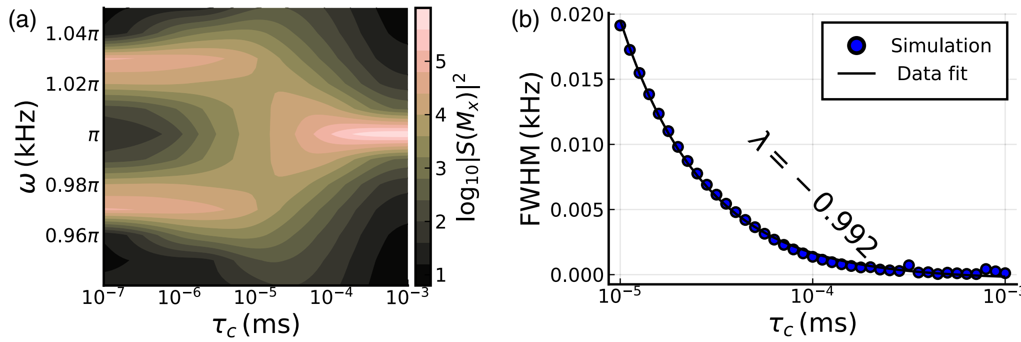

FIG. 7. (a) shows the contour plot of $|S(M_x)|^2$ as a function of τ_c and ω. The list of fixed parameters is given here, $\omega_1 = 2\pi \times 125$ kHz, $\omega_d = 2\pi \times 0.1$ kHz, $\omega_1\tau_1 = 2\pi$, $\omega_2\tau_2 = 1.03\pi$, $N = 15$, and $n = 200$. The DTC phase is more robust in the high τ_c regime as a single narrower peak arises at $\tau_c = 10^{-3}$ ms. For lowering τ_c, the peak becomes broader, and around $\tau_c \rightarrow 10^{-5}$ ms, the single peak breaks into two peaks at $\omega = \pi \pm 0.03\pi$, which leads to the breaking of 2τ periodicity in the system. To find the dependency of τ_c on the broadening, we plot FWHM as a function of τ_c and also fit with $p_2(\tau_c) = a + b\times\tau_c^{\lambda}$ in (b). The list of the fixed parameters is given as (a). The value of the fitting parameters are, $a = -3.6\times10^{-4}$, $b = 2.181\times10^{-7}$, and $\lambda = -0.992$. Hence for higher τ_c, the DTC phase becomes more stable.

decreasing ω_d, the DTC phase becomes more robust. For both cases, the upper bound is given by $\omega_1\tau_c < 1$, and $\omega_d\tau_c < 1$.

We also check the stability of the DTC phase by changing the atom number. To use the $|JM\rangle$ basis for a higher number of atoms, we need an averaged dipolar interaction in the model. Previously, we mentioned that for N number of atoms, the averaged interaction can be modeled as $\omega_d \propto |\omega_{d_{ij}}|/N$, where $\omega_{d_{ij}}$ is the nearest-neighbor interaction. Using the above relation, we numerically plot the time evolution of M_x and its spectrum, which is shown in Fig. 9. Our result implies that for increasing the number of atoms the behavior of the DTC phase remains unchanged as the major contribution is coming from the nearest-neighbor interactions.

V. DISCUSSIONS

To predict the robust period-doubling response, we have used the FRQME for deriving the dynamical equation of the dissipative systems, in the presence of the drive and dipolar interaction [32]. Such formalism predicts unique second-order terms of the above-mentioned interactions, which play a major role in the stability of the DTC phase.

Recently, it has been reported that the interplay between drive and dissipation lead to persistence oscillation, which plays a key role in the emergence of the DTC phase in driven dissipative systems [34,46–49]. For example, due to the imperfect rotation in dissipative-Floquet systems, the system starts to evolve in the wrong sector of the Hilbert space, which is corrected by dissipation, leading to a stable DTC [46]. Similarly, in our case, due to imperfect rotation along the y axis, M_z starts to evolve, which can be stabilized by increasing the dissipation time (τ_1). Therefore, our results support the recent theoretical arguments on the stability of DTC in dissipative systems [46]. However, in the presence of the imperfect rotation δ, such period-doubling response becomes short lived, as the decay rate of the oscillations is proportional to $\delta^{2.267}$, which also matches with the recent experimental observation by Beatrez *et al.* [17].

We also find that in the presence of the perturbation, the spin-locking pulse with a larger time duration is much more effective in diminishing the destructive effect of the perturbation (shown in Fig. 4(c)), which is in agreement with the works by Choi *et al.* [13]. There exists an upper bound of τ_1, as in this high-τ_1 regime the system-bath coupling becomes

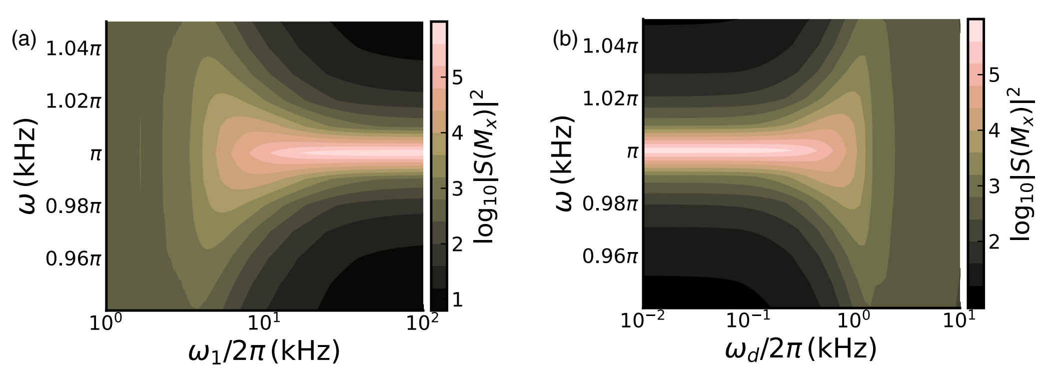

FIG. 8. (a) shows the contour plot of $\log_{10}|S(M_x)|^2$ as a function of ω_1 and ω. The list of fixed parameters is given here, $\tau_1 = 20$ ms, $\omega_d = 2\pi \times 0.1$ kHz, $\omega_2\tau_2 = 1.03\pi$, $\tau_c = 10^{-3}$ ms, $N = 15$, and $n = 200$. For lower values of ω_1, the peak at $\omega = \pi$ becomes broader. On the other hand, for higher values of ω_1, it becomes more robust as we have a narrower peak at $\omega = \pi$, so the DTC phase is more robust in this regime. In (b), we show the contour plot of $\log_{10}|S(M_x)|^2$ as a function of ω_d and ω. The list of fixed parameters is given here, $\omega_1 = 2\pi \times 50$ kHz, $\omega_1\tau_1 = 2\pi$, $\omega_2\tau_2 = 1.03\pi$, $\tau_c = 10^{-3}$ ms, $N = 15$, and $n = 200$. It shows exactly the opposite behavior of Fig. 8(a). As for higher ω_d, the peak at $\omega = \pi$ becomes broader. Hence, the strong dipolar coupling has a negative effect in the DTC phase.

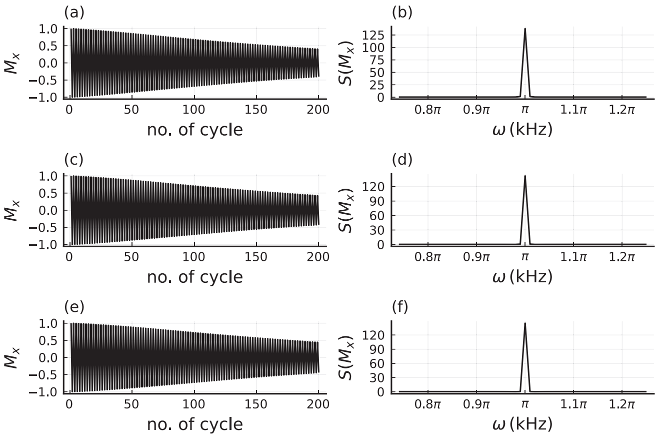

FIG. 9. Plot of M_x versus the number of cycles is shown in (a), (c), (e) and their corresponding Fourier transform, $S(M_x)$ versus ω are shown in (b), (d), and (f). The value of the fixed parameters are given as, $\omega_1 = 2\pi\times 25$ kHz, $|\omega_{d_{ij}}| = 2\pi\times 2$ kHz, $\tau_c = 10^{-3}$ ms, $\omega_1\tau_1 = 2\pi\times 2$, $\omega_2\tau_2 = 1.01\pi$, and $n = 200$. For the top plot [(a), (b)], $N = 15$, $\omega_d = |\omega_{d_{ij}}|/15$ kHz. For the middle plot [(c), (d)], $N = 20$, $\omega_d = |\omega_{d_{ij}}|/20$ kHz. For the bottom plot [(e), (f)], $N = 25$, $\omega_d = |\omega_{d_{ij}}|/25$ kHz. For all the cases, M_x and $S(M_x)$ show nearly the same behavior as the major contribution is coming from the nearest-neighbors interactions ($|\omega_{d_{ij}}| \propto 1/r^3$). Therefore, for increasing the no. of atoms, the DTC phases remain intact. In plots showing spectra in (b), (d), and (f), the y axis is in arbitrary units.

effective, so the system further thermalizes (T_1 process). The upper bound of τ_1 is given by, $\tau_1/T_1 < 1$. As the DTC phase can only be found in the nonequilibrium time domain, such choice of τ_1 is prohibited.

We also check the stability of the DTC phase, by varying the other parameters, ω_1, and ω_d. Such stability depends on the higher values of $M_x(t)$ in the quasistationary prethermal phase. Our results show that a stronger drive is required in this case. Similarly, a much weaker dipolar interaction also plays the same role here. Therefore, the presence of the dipolar interaction contributes to the decay of the prethermal order, as $M_x^{\text{pre}} \propto M_\circ(1 - \frac{9}{16}(\frac{\omega_d}{\omega_1})^2)$ for $\omega_1 > \omega_d$, so the decay rate is proportional to ω_d^2. Such dependency was previously reported by Beatrez *et al.* [17]. We note that, for $\omega_d = 0$, our dynamical equation has similarities with the collective spin Markovian dephasing process $\mathcal{L}_{\text{sec}}[\rho_S] \propto \gamma(2J_x\rho_S J_x - \{J_x^2, \rho_S\})$ [13], which can successfully predict the existence of 2τ periodicity in the x direction. Although, the fundamental difference between the two processes is given as, in our case $\gamma \propto \omega_1^2\tau_c$, and only FRQME can predict such processes, which is known as drive-induced dissipation (DID) [32]. On the other hand, for the dephasing process $\gamma \propto \omega_{\text{SL}}^2\frac{\tau_c}{1+(\omega_\circ\tau_c)^2}$, as $\omega_1 \gg \omega_{\text{SL}}$, such process is neglected in this case. In the experiment, spins are randomly oriented in the absence of dipolar interaction, such random configuration of the spins provides a detrimental effect to the DTC phase. Therefore, $\omega_1 > \omega_d \gg \omega_{\text{SL}} > 0$ is the necessary condition for having a stable DTC phase.

We also note that the $1/r^3$ dependence of the dipolar interaction implies that, the major contribution is coming from the nearest-neighbor interactions. Therefore, in the case of a multispin dipolar network, if we assume that the coupling amplitude between the spin pairs is equal, without proper averaging of such interactions, we get a period-doubling response with a higher decay rate. As the effective interaction between the nearest spin pairs increases without the averaging. Such issue can be resolved by assuming $\omega_d \propto \omega_{d_{ij}}/N$ [45].

Our prescription can be extended to any number of dipolar coupled spins in an ensemble. There exist other methods based on a mean-field quantum master equation for observing the persistent period-doubling oscillations in open many-body quantum systems [34,35]. We note that our approach has significant differences from the previous methods and matches well with the existing experimental pieces of evidence [13,17].

For the dissipative dipolar systems, the subharmonic response in the presence of a long-lived prethermal phase has some dissimilarities from the usual definition of the Floquet time crystal as proposed by Else *et al.* [33]. In the former case, the period-doubling response is not long lived and it depends on the lifetime of the prethermal plateau [17]. In addition to that, due to the presence of self-averaging effects, the experimental results for nearly 10^3 number of spins can be theoretically reproduced using only fewer atoms, which we confirm using our analytical and numerical results. On the other hand, for the Floquet time crystal, the robust subharmonic response is only possible in the thermodynamic limit of the atoms. A brief discussion on the difference between the experimentally found prethermal DTC and the Floquet DTC is also provided in the review article by Khemani *et al.* [7].

Moreover, we find that the DTC phase depends on the environmental parameter (τ_c), which in turn suggests that the DTC phase is more stable at low temperatures. We also note that FRQME has a region of validity as too low temperature might break the timescale separation argument, requiring a non-Markovian approach.

VI. CONCLUSIONS

As a summary, using FRQME, we have provided an alternative theoretical explanation for the emergence of the prethermal DTC phase in a dissipative dipolar network experiencing the two-pulse excitation (i.e., the spin-locking pulse followed by a rotation in the perpendicular direction). We note that, during the evolution under the spin-locking pulse, a quasiconserved quantity exists, which plays a pivotal role in preserving the prethermal order. We show that the robustness of the DTC phase depends on the long-lived prethermal order. We also check the stability of the DTC phase by changing the existing parameters in our dynamical equation, and we note that our analytical and numerical results also match with the recent experimental works. In addition, we find that such period-doubling oscillations are more robust at the lower temperature. We envisage that our approach will be useful in quantum synchronization problems. Moreover, our analysis can also be extended to describe other kinds of exotic nonequilibrium phases that emerged in the driven dissipative many-body systems.

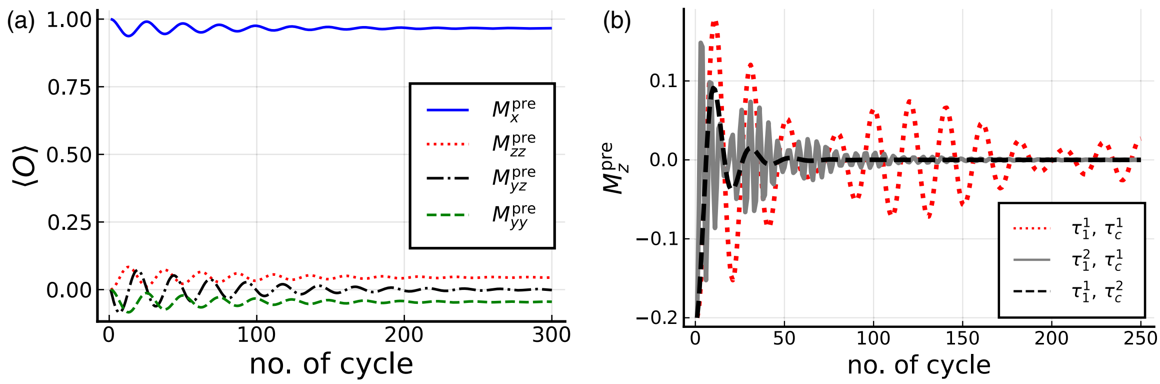

FIG. 10. (a) shows the plot of observables ($\langle O\rangle$), which are, $M_x^{\rm pre}$ (blue solid line, the top curve), $M_{zz}^{\rm pre}$ (red dotted line, second from the top), $M_{yy}^{\rm pre}$ (green dashed line, the bottom curve), and $M_{yz}^{\rm pre}$ (black dash-dotted line, second from the bottom) versus number of cycle by numerically solving Eq. (7). Here, $\omega_2\tau_2 = 0$. The list of fixed parameters are given as, $\omega_1 = 2\pi\times 40$ kHz, $\omega_{d_0} = 2\pi\times 10$ kHz, $\tau_c = 10^{-4}$ ms, and $\omega_1\tau_1 = 2\pi\times 0.02$. The initial condition is chosen as $M_x|_{t\to 0} = 1$. For such a choice of parameters, the system reaches a steady state after some cycle. The dynamical evolution of $M_{zz}^{\rm pre}$, $M_{yy}^{\rm pre}$, $M_{yz}^{\rm pre}$ are negligible compared to $M_x^{\rm pre}$. (b) shows the plot of observables $M_z^{\rm pre}$ versus the number of cycles for three different choices of τ_1, τ_c. Here $\omega_2\tau_2 = 0$. The list of fixed parameters are $\omega_1 = 2\pi\times 40$ kHz, $\omega_{d_0} = 2\pi\times 4$ kHz. Three choices are given as $\{\omega_1\tau_1^1 = 2\pi\times 0.05,\ \tau_c^1 = 10^{-4}$ ms$\}$ (red dotted line), $\{\omega_1\tau_1^2 = 2\pi\times 0.2,\ \tau_c^1 = 10^{-4}$ ms$\}$ (gray solid line), and $\{\omega_1\tau_1^1 = 2\pi\times 0.05,\ \tau_c^2 = 10^{-3}$ ms$\}$ (black dashed line). The initial condition is chosen as $M_z|_{t\to 0} = -0.2$. The above plot indicates that for higher values of τ_c and τ_1, $M_z^{\rm pre}$ decays faster for increasing the number of cycles. Such a condition is necessary for obtaining the DTC phase.

ACKNOWLEDGMENTS

The authors thank Arpan Chatterjee for his insightful comments and helpful suggestions. S.S. gratefully acknowledges University Grants Commission (UGC) of the Government of India for a senior research fellowship (SRF) (Reference ID: MAY2018-528071).

APPENDIX: DYNAMICS UNDER SPIN-LOCKING SEQUENCE

The dynamical equation under the spin-locking sequence is given by,

$$\frac{d\rho_S}{dt} = -i[H_{\rm sec}, \rho_S] - \tau_c[H_{\rm sec}, [H_{\rm sec}, \rho_S]], \tag{A1}$$

Here, $H_{\rm sec} = H_x^{\rm sec} + H_{\rm dd}^{\rm sec}$. The representation of the symmetric observables is given by,

$$\begin{aligned} M_\alpha &= {\rm Tr}_s[(I_\alpha\otimes\mathbb{I} + \mathbb{I}\otimes I_\alpha)\rho_s] \\ M_{\alpha\beta} &= {\rm Tr}_s[(I_\alpha\otimes I_\beta + I_\beta\otimes I_\alpha)\rho_s], \quad \forall\,\alpha\neq\beta \\ M_{\alpha\alpha} &= {\rm Tr}_s[(I_\alpha\otimes I_\alpha)\rho_s]. \end{aligned}\tag{A2}$$

Here, $\alpha,\beta\in\{x,y,z\}$. In the presence of $H_{\rm sec}$, the dynamical equations can be divided into two subgroups. Each group contains four observables, $\{M_x, M_{yy}, M_{zz}, M_{yz}\}$ and $\{M_y, M_z, M_{xy}, M_{xz}\}$. The dynamical equations for the first group are given by,

$$\begin{aligned}\dot{M}_x = &-\tfrac{9}{4}\omega_{d_0}^2\tau_c M_x + 6\omega_1\omega_{d_0}\tau_c M_{zz} - 6\omega_1\omega_{d_0}\tau_c M_{yy} \\ &- 3\omega_{d_0}M_{yz}\end{aligned}\tag{A3}$$

$$\dot{M}_{zz} = \tfrac{3}{4}\omega_1\omega_{d_0}\tau_c M_x - 2\omega_1^2\tau_c M_{zz} + 2\omega_1^2\tau_c M_{yy} + \omega_1 M_{yz} \tag{A4}$$

$$\dot{M}_{yy} = -\tfrac{3}{4}\omega_1\omega_{d_0}\tau_c M_x + 2\omega_1^2\tau_c M_{zz} - 2\omega_1^2\tau_c M_{yy} - \omega_1 M_{yz} \tag{A5}$$

$$\begin{aligned}\dot{M}_{yz} = &\tfrac{3}{4}\omega_{d_0}M_x - 2\omega_1 M_{zz} + 2\omega_1 M_{yy} \\ &- \left(4\omega_1^2 + \tfrac{9}{4}\omega_{d_0}^2\right)\tau_c M_{yz}.\end{aligned}\tag{A6}$$

There exist several conserved quantities in this block, which are given by,

$$3\omega_{d_0}\dot{M}_{zz} + \omega_1\dot{M}_x = 0 \tag{A7}$$

$$\dot{M}_{yy} + \dot{M}_{zz} = 0 \tag{A8}$$

$$\dot{M}_{xx} = 0. \tag{A9}$$

For the demonstration of the DTC phase, the loss of x magnetization must be very small in each cycle of the evolution. Otherwise, $M_x(t)$ will vanish after a few cycles. Such condition will be satisfied if $\omega_1 > \omega_d$. From the below plot (Fig. 10), the evolution of $\{M_{zz}, M_{yy}, M_{yz}\}$ are negligible compared to M_x in the limit $\omega_1 > \omega_d$. The dynamical equations for the other group are written as,

$$\dot{M}_z = -\omega_1^2\tau_c M_z + \omega_1 M_y + 3\omega_1\omega_{d_0}\tau_c M_{xz} \tag{A10}$$

$$\dot{M}_y = -\omega_1 M_z - \left(\omega_1^2 + \tfrac{9}{4}\omega_{d_0}^2\right)\tau_c M_y + 3\omega_{d_0}M_{xz} + 3\omega_1\omega_{d_0}\tau_c M_{xy} \tag{A11}$$

$$\dot{M}_{xz} = \tfrac{3}{4}\omega_1\omega_{d_0}\tau_c M_z - \tfrac{3}{4}\omega_{d_0}M_y - \left(\omega_1^2 + \tfrac{9}{4}\omega_{d_0}^2\right)\tau_c M_{xz} + \omega_1 M_{xy} \tag{A12}$$

$$\dot{M}_{xy} = \tfrac{3}{4}\omega_1\omega_{d_0}\tau_c M_y - \omega_1 M_{yz} - \omega_1^2\tau_c M_{xy}. \tag{A13}$$

As there exist no conserved quantities involving the observables from this group, all the observables will vanish at the steady state even if they have any initial nonzero values. There is no closed analytical form for the observables. Hence we provide the plot of the observable $M_z^{\mathrm{pre}}(M_\alpha, t)$ by numerically solving Eqs. (A10)–(A13) for a different choice of $\tau_1,\ \tau_c$. Here, $M_z|_{t\to 0} = M_\alpha$. Other observables are not relevant for this case.

[1] A. Polkovnikov, K. Sengupta, A. Silva, and M. Vengalattore, Rev. Mod. Phys. **83**, 863 (2011).

[2] J. Eisert, M. Friesdorf, and C. Gogolin, Nat. Phys. **11**, 124 (2015).

[3] D. A. Abanin and Z. Papić, Ann. Physik **529**, 1700169 (2017).

[4] M. Ueda, Nat. Rev. Phys. **2**, 669 (2020).

[5] N. Y. Yao, A. C. Potter, I.-D. Potirniche, and A. Vishwanath, Phys. Rev. Lett. **118**, 030401 (2017).

[6] K. Sacha and J. Zakrzewski, Rep. Prog. Phys. **81**, 016401 (2018).

[7] V. Khemani, R. Moessner, and S. L. Sondhi, arXiv:1910.10745.

[8] P. Bruno, Phys. Rev. Lett. **111**, 070402 (2013).

[9] H. Watanabe and M. Oshikawa, Phys. Rev. Lett. **114**, 251603 (2015).

[10] V. Khemani, A. Lazarides, R. Moessner, and S. L. Sondhi, Phys. Rev. Lett. **116**, 250401 (2016).

[11] D. V. Else, B. Bauer, and C. Nayak, Phys. Rev. Lett. **117**, 090402 (2016).

[12] J. Zhang, P. W. Hess, A. Kyprianidis, P. Becker, A. Lee, J. Smith, G. Pagano, I.-D. Potirniche, A. C. Potter, A. Vishwanath, N. Y. Yao, and C. Monroe, Nature (London) **543**, 217 (2017).

[13] S. Choi, J. Choi, R. Landig, G. Kucsko, H. Zhou, J. Isoya, F. Jelezko, S. Onoda, H. Sumiya, V. Khemani, C. von Keyserlingk, N. Y. Yao, E. Demler, and M. D. Lukin, Nature (London) **543**, 221 (2017).

[14] J. Rovny, R. L. Blum, and S. E. Barrett, Phys. Rev. Lett. **120**, 180603 (2018).

[15] S. Pal, N. Nishad, T. S. Mahesh, and G. J. Sreejith, Phys. Rev. Lett. **120**, 180602 (2018).

[16] A. Kyprianidis, F. Machado, W. Morong, P. Becker, K. S. Collins, D. V. Else, L. Feng, P. W. Hess, C. Nayak, G. Pagano, N. Y. Yao, and C. Monroe, Science **372**, 1192 (2021).

[17] W. Beatrez, C. Fleckenstein, A. Pillai, E. de Leon Sanchez, A. Akkiraju, J. Diaz Alcala, S. Conti, P. Reshetikhin, E. Druga, M. Bukov, and A. Ajoy, Nat. Phys. **19**, 407 (2023).

[18] H. Keßler, P. Kongkhambut, C. Georges, L. Mathey, J. G. Cosme, and A. Hemmerich, Phys. Rev. Lett. **127**, 043602 (2021).

[19] Z. Gong, R. Hamazaki, and M. Ueda, Phys. Rev. Lett. **120**, 040404 (2018).

[20] H. Taheri, A. B. Matsko, L. Maleki, and K. Sacha, Nat. Commun. **13**, 848 (2022).

[21] W. W. Ho, S. Choi, M. D. Lukin, and D. A. Abanin, Phys. Rev. Lett. **119**, 010602 (2017).

[22] W. Beatrez, O. Janes, A. Akkiraju, A. Pillai, A. Oddo, P. Reshetikhin, E. Druga, M. McAllister, M. Elo, B. Gilbert, D. Suter, and A. Ajoy, Phys. Rev. Lett. **127**, 170603 (2021).

[23] T. Kuwahara, T. Mori, and K. Saito, Ann. Phys. (NY) **367**, 96 (2016).

[24] M. Bukov, S. Gopalakrishnan, M. Knap, and E. Demler, Phys. Rev. Lett. **115**, 205301 (2015).

[25] A. Rubio-Abadal, M. Ippoliti, S. Hollerith, D. Wei, J. Rui, S. L. Sondhi, V. Khemani, C. Gross, and I. Bloch, Phys. Rev. X **10**, 021044 (2020).

[26] C. Yin, P. Peng, X. Huang, C. Ramanathan, and P. Cappellaro, Phys. Rev. B **103**, 054305 (2021).

[27] M. Holthaus, J. Phys. B: At. Mol. Opt. Phys. **49**, 013001 (2016).

[28] D. A. Abanin, W. De Roeck, and F. Huveneers, Phys. Rev. Lett. **115**, 256803 (2015).

[29] P. Peng, C. Yin, X. Huang, C. Ramanathan, and P. Cappellaro, Nat. Phys. **17**, 444 (2021).

[30] S. Saha and R. Bhattacharyya, Phys. Rev. A **107**, 022206 (2023).

[31] A. Chakrabarti and R. Bhattacharyya, Europhys. Lett. **142**, 55001 (2023).

[32] A. Chakrabarti and R. Bhattacharyya, Phys. Rev. A **97**, 063837 (2018).

[33] D. V. Else, B. Bauer, and C. Nayak, Phys. Rev. X **7**, 011026 (2017).

[34] F. M. Gambetta, F. Carollo, M. Marcuzzi, J. P. Garrahan, and I. Lesanovsky, Phys. Rev. Lett. **122**, 015701 (2019).

[35] M. Krishna, P. Solanki, M. Hajdušek, and S. Vinjanampathy, Phys. Rev. Lett. **130**, 150401 (2023).

[36] F. Iemini, A. Russomanno, J. Keeling, M. Schirò, M. Dalmonte, and R. Fazio, Phys. Rev. Lett. **121**, 035301 (2018).

[37] C. Slichter, *Principles of Magnetic Resonance*, Springer Series in Solid-State Sciences (Springer, Berlin, 1996).

[38] A. Chakrabarti and R. Bhattacharyya, Europhys. Lett. **121**, 57002 (2018).

[39] F. P. Heinz-Peter Breuer, *The Theory of Open Quantum Systems* (Oxford University Press, Oxford, 2002).

[40] N. Chanda and R. Bhattacharyya, Phys. Rev. A **101**, 042326 (2020).

[41] A. Chatterjee and R. Bhattacharyya, Phys. Rev. A **102**, 043111 (2020).

[42] N. Chanda and R. Bhattacharyya, Phys. Rev. A **104**, 022436 (2021).

[43] S. Saha and R. Bhattacharyya, J. Magn. Reson. Open **10–11**, 100046 (2022).

[44] S. Saha and R. Bhattacharyya, J. Phys. B: At. Mol. Opt. Phys. **55**, 235501 (2022).

[45] S. Lacelle and L. Tremblay, J. Chem. Phys. **98**, 3642 (1993).

[46] A. Lazarides, S. Roy, F. Piazza, and R. Moessner, Phys. Rev. Res. **2**, 022002(R) (2020).

[47] B. Buča, J. Tindall, and D. Jaksch, Nat. Commun. **10**, 1730 (2019).

[48] G. Passarelli, P. Lucignano, R. Fazio, and A. Russomanno, Phys. Rev. B **106**, 224308 (2022).

[49] S. Sarkar and Y. Dubi, Commun. Phys. **5**, 155 (2022).